Electromagnetic properties of ^{21}O for benchmarking nuclear Hamiltonians

S. Heil [a], M. Petri [b,a,*], K. Vobig [a], D. Bazin [c,d], J. Belarge [c,1], P. Bender [c,e], B.A. Brown [c,d], R. Elder [c,d], B. Elman [c,d], A. Gade [c,d], T. Haylett [b], J.D. Holt [f], T. Hüther [a], A. Hufnagel [a], H. Iwasaki [c,d], N. Kobayashi [c], C. Loelius [c,d], B. Longfellow [c,d], E. Lunderberg [c,d], M. Mathy [a], J. Menéndez [g], S. Paschalis [b], R. Roth [a], A. Schwenk [a,h,i], J. Simonis [a], I. Syndikus [a], D. Weisshaar [c], K. Whitmore [c,d]

[a] *Institut für Kernphysik, Technische Universität Darmstadt, 64289 Darmstadt, Germany*
[b] *Department of Physics, University of York, Heslington, York, YO10 5DD, UK*
[c] *National Superconducting Cyclotron Laboratory, Michigan State University, East Lansing, MI 48824, USA*
[d] *Department of Physics and Astronomy, Michigan State University, East Lansing, MI 48824, USA*
[e] *Department of Physics, University of Massachusetts Lowell, Lowell, MA 01854, USA*
[f] *TRIUMF 4004 Wesbrook Mall, Vancouver, British Columbia V6T 2A3, Canada*
[g] *Center for Nuclear Study, The University of Tokyo, Tokyo, Japan*
[h] *ExtreMe Matter Institute EMMI, GSI Helmholtzzentrum für Schwerionenforschung GmbH, 64291 Darmstadt, Germany*
[i] *Max-Planck-Institut für Kernphysik, 69117 Heidelberg, Germany*

ARTICLE INFO

ABSTRACT

The structure of exotic nuclei provides valuable tests for state-of-the-art nuclear theory. In particular electromagnetic transition rates are more sensitive to aspects of nuclear forces and many-body physics than excitation energies alone. We report the first lifetime measurement of excited states in ^{21}O, finding $\tau_{1/2^+} = 420^{+35}_{-32}(\text{stat})^{+34}_{-12}(\text{sys})$ ps. This result together with the deduced level scheme and branching ratio of several γ-ray decays are compared to both phenomenological shell-model and ab initio calculations based on two- and three-nucleon forces derived from chiral effective field theory. We find that the electric quadrupole reduced transition probability of $B(E2; 1/2^+ \rightarrow 5/2^+_{\text{g.s.}}) = 0.71^{+0.07}_{-0.06}{}^{+0.02}_{-0.06}$ e^2 fm^4, derived from the lifetime of the $1/2^+$ state, is smaller than the phenomenological result where standard effective charges are employed, suggesting the need for modifications of the latter in neutron-rich oxygen isotopes. We compare this result to both large-space and valence-space ab initio calculations, and by using multiple input interactions we explore the sensitivity of this observable to underlying details of nuclear forces.

Understanding nuclear structure and dynamics in terms of the fundamental interactions between protons and neutrons is one of the overarching goals of nuclear science. To this end, nuclear theory is developing chiral effective field theory (EFT) [1,2], a unified approach to nuclear forces, where two-nucleon (NN), three-nucleon (3N) and higher-body forces are derived within a consis-

tent, systematically improvable framework. This approach coupled with parallel advances in ab initio many-body theory [3–8] provides the possibility to link the structure of nuclei to the underlying symmetries of quantum chromodynamics.

Neutron-rich oxygen isotopes are particularly fruitful candidates to test ab initio theory at the interface of the light- and medium-mass regions. Due to their semi-magic nature, most oxygen isotopes are accessible to many-body approaches amenable to heavier systems, while still being light enough to be treated in quasi-exact methods, such as extensions of the no-core shell model (NCSM). First valence-space calculations with NN+3N forces were able to explain, for the first time, the location of the oxygen dripline at ^{24}O [9]. More recently, large-space ab initio calculations, where all nucleons are treated as explicit degrees of freedom, have con-

firmed those early results [10,11,5] and new calculations have even extended dripline predictions to the entire region [12]. Furthermore excitation spectra in oxygen have also been obtained with NN+3N forces, generally yielding agreement with experiment approaching that of state-of-the-art phenomenology [13–16]. An important next step is to benchmark ab initio theory against other observables which are sensitive to physics beyond what is relevant for excitation energies alone. For instance the long-standing problem of quenching of beta decays across the nuclear chart has recently been explained [17], but electromagnetic properties have only been intermittently studied [18–22]. Indeed, very limited or no data exists for transition rates in the neutron-rich oxygen isotopes. In ^{21}O, in particular, no experimental information is available on transition rates, while γ decays from bound excited states beyond the first have been reported in [23] with very limited statistics. Therefore, we performed an experiment which had the goal to extract for the first time electromagnetic transition rates and branching ratios in ^{21}O, in order to benchmark and critically test state-of-the-art nuclear structure theories.

In this Letter, we report first electromagnetic transition rates from low-lying excited states of ^{21}O. We compare our results to predictions from phenomenological shell model and two ab initio many-body methods, the in-medium (IM-) NCSM and the valence-space in-medium similarity renormalization group (VS-IMSRG). Using a number of chiral EFT NN+3N forces, we study the sensitivity of electromagnetic transitions to details of nuclear interactions. It should be noted that electromagnetic two-body currents, currently under development, are not included in the ab initio calculations.

The experiment was performed at the National Superconducting Cyclotron Laboratory (NSCL) at Michigan State University. A ^{24}F secondary beam was produced by fragmenting a 140 MeV/nucleon ^{48}Ca beam on a 893 mg/cm^2 ^{9}Be production target. The A1900 separator [24,25] was used to select and transport the ^{24}F ions (with an energy of 95 MeV/nucleon, a 2.5% momentum dispersion and 95% purity) to the experimental vault where they underwent reactions on a secondary 2 mm ^{9}Be target, located at the target position of the S800 spectrograph [26]. ^{21}O was produced via the ^{9}Be(^{24}F,^{21}O+γ)X multi-nucleon removal reaction and identified on an event-by-event basis via energy-loss and time-of-flight measurements. Emitted γ rays were detected with the Gamma-Ray Energy Tracking In-beam Nuclear Array (GRETINA) [27,28].

Data were recorded with two different settings: I) the secondary ^{9}Be target was solely used, and II) a 0.92 mm ^{181}Ta degrader was mounted at distances of 25 mm (II/25) or 45 mm (II/45) downstream of the target using the TRIple PLunger for EXotic beams [29]. The velocity of the ^{21}O fragments was $v/c \approx 0.41$ after the target and $v/c \approx 0.36$ after the degrader. To maximize the sensitivity and efficiency of GRETINA, the target position was moved upstream by 13 cm for setting I and II/25, covering angles between 20° to 70°, and by an additional 20 mm for setting II/45. The tracking capabilities of GRETINA were used to determine the interaction sequence and thus the detection angle of the γ rays used for the Doppler correction. The trajectory of the outgoing ^{21}O fragments was measured with S800 and their determined angles and momenta were employed in the Doppler correction on an event-by-event basis.

To determine the lifetime of the ^{21}O $1/2^+$ state, its γ-ray decay to the $5/2^+$ ground state has been analysed using data from settings I and II. In setting I, the lifetime is inferred from the low-energy tail that is generated in the γ-ray spectrum, see Fig. 1(a). This tail results from nuclear levels decaying farther away from the target, but being Doppler corrected as if they decay promptly at the target position, see, e.g., [30–33]. In setting II, the Recoil Distance Method (RDM) was employed, where γ rays emitted before or after the degrader experience different Doppler shifts leading
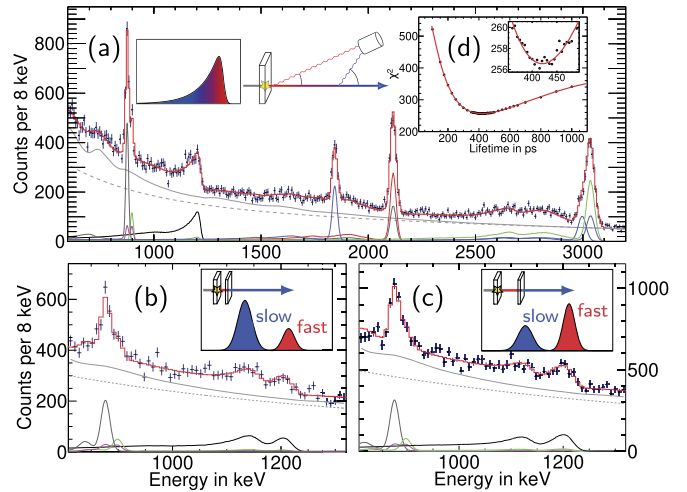

Fig. 1. Comparison of experimental γ-ray spectra to simulations for $\tau_{1/2^+} = 420$ ps in settings (a) I, (b) II/25 and (c) II/45. Simulations for different cascades are shown in varying colours. The laboratory-frame background (grey, solid) is shown on top of a double exponential background (grey, dashed). The sum of all simulated spectra (red) has been fitted to the data (blue). The insets illustrate the spectral features of the lifetime measurements. (d) Un-normalized χ^2 distribution for $\tau_{1/2^+}$, combined for all settings, with a feeding lifetime of $\tau_{3/2^+} = 8$ ps and DRR = 22.6%, and fitted with a fourth-order polylogarithmic function. The inlay zooms around the minimum of the distribution, with a reduced $\chi^2 \approx 1$ (Neyman χ^2 with 265 degrees-of-freedom).

to two laboratory energies, typically called the fast and slow component of the peak in the γ-ray spectrum, as can be seen in the insets of Fig. 1(b) and (c). The ratio of the number of γ rays in the fast and slow peak infers the lifetime of the state. The RDM for fast beams and its implementation at the NSCL is described in [33–38]. Since reactions populating the state of interest occur also in the degrader, the degrader-reaction ratio (DRR) has to be taken into account when evaluating the fast and slow components in an RDM measurement. The DRR has been determined by evaluating γ-ray transitions with much shorter lifetimes. Since the production mechanism is a multi-nucleon removal reaction, the DRR is assumed to be similar for all transitions.

To determine the lifetime, branching ratios and DRR, the measurements are compared to simulations obtained with Geant4 [39], simulating all relevant properties, i.e., detector geometry and response, γ-ray cascades, lifetimes, beam profile [34]. The energy of the $1/2^+$ state is taken as 1221.5 ± 2.2 keV, the average from two β-decay experiments [40,41]. The energies of the remaining levels are determined from the data. The experimentally obtained level scheme for ^{21}O is shown in Fig. 2. All cascades are simulated separately, as well as the neutron induced background from Ge(n, n') and Al(n, X) reactions in GRETINA and the beam-line, respectively. The neutron induced background is simulated as a combination of non-moving γ-ray sources at the target position with the respective energies, where the intensities are obtained from the data. This background is then Doppler corrected and added to the experimental background. The obtained spectra are summed up with separate normalization factors for each simulation. Finally the summed spectrum is modified by a double-exponential background and fitted to the measured spectra using the least-squares method. The free parameters are hereby given by the exponential background, the normalization factor for each setting, and the relative strengths of each of the simulated cascades. The minimization is performed with all parameters free over the full energy range for all settings simultaneously. Such simulations are then performed for various DRRs and a χ^2 minimization is performed determining DRR = 22.6% $\pm$ 1.8%. Using the data from settings I and II and the determined DRR, the lifetime of the $1/2^+$ state is extracted
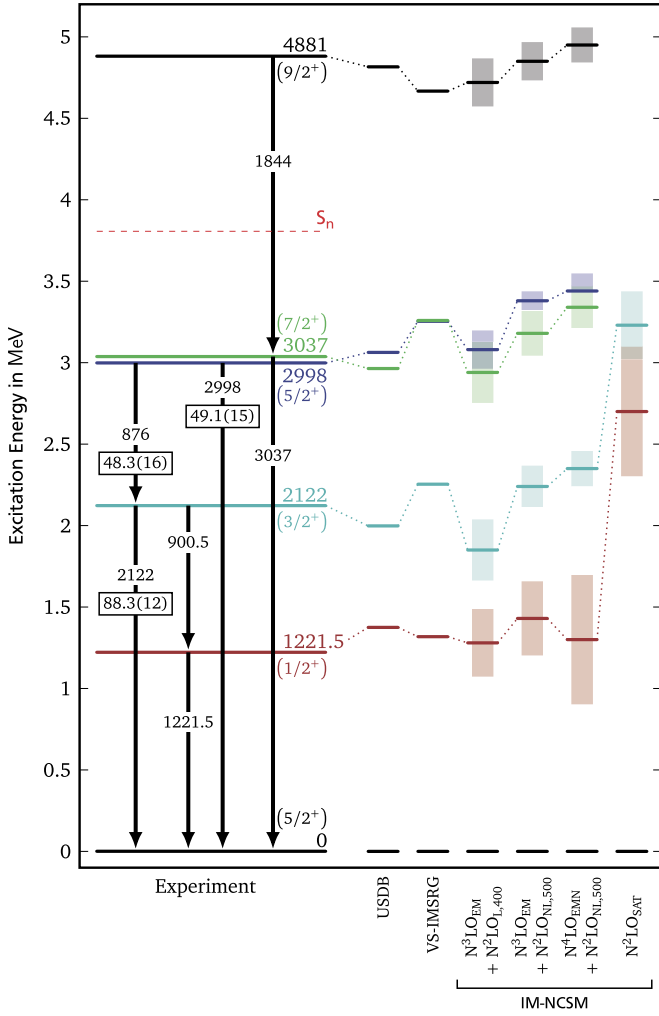
Fig. 2. Level scheme of ^{21}O determined in this experiment and how this compares to IM-NCSM with four different chiral NN+3N interactions (see text for details), VS-IMSRG, and phenomenological shell model with $e_n = 0.45$. Experimental branching ratio (in %) of γ-ray decays are marked in rectangles. The 3037 and 1844 keV γ-ray transitions are in coincidence, as well as the 876 and 2122 keV, placing them firmly on the level scheme. The 900.5 keV transition has been observed for the first time, allowing the determination of the γ-ray decay branching ratio of the 2122 keV level. Ordering of the $(5/2^+)$ and $(7/2^+)$ states at 3 MeV has been based on γ-ray branching-ratio consideration. The coloured bands represent theoretical uncertainties (see text for details).

as $\tau_{1/2^+} = 420^{+35}_{-32}(\text{stat})^{+34}_{-12}(\text{sys})\,\text{ps}$ in an equivalent minimization process as described for the DRR, resulting in the χ^2 distribution shown in Fig. 1(d). The χ^2 is calculated between 1050 keV and 1260 keV, covering both the full peak and tail for setting I, as well as both fast and slow peaks for settings II. The statistical uncertainty is given by the un-normalized $\chi^2_{min} + 1$ range, while the systematic uncertainty is dominated by the uncertainty of the DRR and the energy of the first excited state. To construct a consistent level scheme from the measured γ-ray energies, the lifetime of the $3/2^+$ state is determined via the centroid-shift method, see, e.g., [32,42], to $\tau_{3/2^+} = 8^{+21}_{-8}$ ps.

We compare the experimental results to phenomenological shell model, and two ab initio methods using chiral EFT NN+3N interactions, the VS-IMSRG and the IM-NCSM, see Figs. 2, 3 and Table 1.

Within the phenomenological shell model, the electric quadrupole transition strengths, B(E2), are obtained with the USDB sd-shell Hamiltonian including the neutron $1d_{5/2}$, $2s_{1/2}$, and $1d_{3/2}$ single-particle orbitals [43]. The E2 matrix elements are calculated
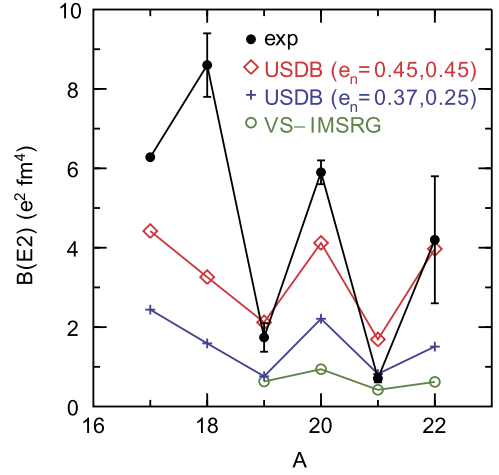

Fig. 3. Experimental B(E2) transition strengths for neutron-rich oxygen isotopes [52,53] and how this compares with the shell model and VS-IMSRG results. For even and odd isotopes the $2^+ \to 0^+$ and $1/2^+ \to 5/2^+$ transition is considered, respectively.

with harmonic-oscillator radial wavefunctions, and with an effective neutron charge $e_n = 0.45$, obtained from a fit to experimental B(E2) values of sd-shell nuclei ($A = 17 - 38$) [44]. The overestimated B(E2) strength in ^{21}O compared to experiment (see Table 1, Fig. 3) shows that the neutron effective charge is smaller than the average value for the sd shell ($e_n = 0.45$). The reason for this was discussed in [45] in terms of microscopic core-polarization[2] models for the effective charge, the latter being orbital and mass dependent. For ^{21}O the $1/2^+$ to $5/2^+$ transition is dominated by the neutron $1d - 2s$ one-body transition density. In [45] the effective charges were calculated with harmonic-oscillator radial wavefunctions for the valence neutrons with the results given in Table 1 of [45]; 0.374 for $1d - 1d$ and 0.248 for $1d - 2s$.[3] The reason for the smaller effective charge for $1d - 2s$, is that the $1d - 2s$ valence transition density has a node near 3.2 fm, see Fig. 1c of [45], resulting in a reduced overlap with the microscopic collective transition density of the core protons, see Fig. 1b of [45]. If these reduced effective charges are used for the calculations, the transition strength for ^{21}O is reduced to B(E2) = 0.82 e^2 fm^4 and agrees with experiment (see Fig. 3). For comparison, if one uses the more realistic Woods-Saxon radial wavefunctions for the valence neutrons, the core-polarization integrals $\langle k(r) \rangle$ are reduced by factors of 0.873 for $1d - 1d$ and 0.688 for $1d - 2s$ (the last column of Table 5 in [45]). The shell-model results for $Z = 8, A = 17 - 22$ are compared to experiment in Fig. 3. Our interpretation of these results is that the wavefunctions for the isotopes closer $N = Z$ require the introduction of two-particle two-hole (2p2h) proton excitations from the core. Indeed, for nuclei close to ^{16}O, and in particular for ^{18}O, the experimental B(E2) values are larger than those calculated, due to the mixing with low-lying states coming from the excitation of protons from the p shell to the sd shell [45]. Therefore, no conclusions regarding effective charges for the sd shell can be drawn by looking at oxygen isotopes closer to stability and a discrepancy between calculated and experimental B(E2) strengths is indeed expected. The experimental state that is dominated by 2p2h proton excitations from the p to the sd shell is at 3.63 MeV for ^{18}O (see Table 1 in [47]) and at 4.46 MeV for ^{20}O (see Fig. 1 in

---

[2] The core polarization takes into account the admixture of one-particle one-hole proton excitations across two major oscillator shells (in this case $1s$ to $2s1d$ and $1p$ to $2p1f$).

[3] These values are in reasonable agreement with recent calculations based on the FTDA model of about 0.33 ($1d_{5/2} - 1d_{5/2}$) and 0.23 ($1d_{5/2} - 2s_{1/2}$) for ^{22}O [46].

Table 1

Comparison of experiment and theory. The experimental B(E2) strength is deduced from the lifetime (τ) of the state. The theoretical branching ratio (BR) is derived using the theoretical B(E2) and B(M1) values and the experimental transition energies. The theoretical $\tau_{1/2^+}$ is calculated using the experimental transition energy. The errors quoted for the IM-NCSM results reflect the uncertainties of the many-body method quantified through a variation of the calculation scheme and model-space size (see text). For the VS-IMSRG, we would expect the theoretical uncertainties from the many-body convergence to be similar to the IM-NCSM calculations, but did not perform a detailed analysis.

	τ [ps]	BR [%]	B(E2) [e^2 fm^4]			B(M1) [$10^{-3}\mu_N^2$]	
	$\frac{1}{2}^+$	$\frac{3}{2}^+ \to \frac{1}{2}^+$	$\frac{1}{2}^+ \to \frac{5}{2}^+$ gs	$\frac{3}{2}^+ \to \frac{1}{2}^+$	$\frac{3}{2}^+ \to \frac{5}{2}^+$ gs	$\frac{3}{2}^+ \to \frac{1}{2}^+$	$\frac{3}{2}^+ \to \frac{5}{2}^+$ gs
Experiment	$420^{+35\ +34}_{-32\ -12}$	11.7 ± 1.2	$0.71^{+0.07\ +0.02}_{-0.06\ -0.06}$				
USDB	176	20.3	1.69	2.06	3.54	5.6	0.6
VS-IMSRG	704	12.7	0.42	0.61	0.55	5.3	2.6
N^{2}LO$_{SAT}$	444^{+128}_{-81}	$4.6^{+5.5}_{-2.6}$	0.67 ± 0.15	0.63 ± 0.05	0.70 ± 0.06	3.0 ± 1.2	4.6 ± 1.9
N^{3}LO$_{EM}$+N^{2}LO$_{L,400}$	804 ± 22	$12.5^{+3.2}_{-2.5}$	0.37 ± 0.01	0.47 ± 0.05	0.55 ± 0.02	9.8 ± 1.0	5.1 ± 0.8
N^{3}LO$_{EM}$+N^{2}LO$_{NL,500}$	488 ± 25	$14.1^{+2.4}_{-1.9}$	0.61 ± 0.03	0.74 ± 0.08	0.77 ± 0.04	8.4 ± 0.4	3.7 ± 0.5
N^{4}LO$_{EMN}$+N^{2}LO$_{NL,500}$	513^{+94}_{-69}	15.5 ± 1.3	0.58 ± 0.09	0.70 ± 0.07	0.77 ± 0.06	8.2 ± 0.5	3.2 ± 0.1

[48]). These intruder states, that have very large B(E2) strengths, mix with the valence neutron configurations. In the model of [49] the energy of the pure two-proton excitations increases with mass; 3.4 MeV for ^{18}O, 4.4 MeV for ^{20}O and 7.8 MeV for ^{22}O. Thus as one adds neutrons, the valence sd neutron configuration should become more dominant. In this interpretation, the heaviest oxygen isotopes have the most pure sd-shell neutron configurations, with the consequence that the B(E2) strength becomes smaller and in better agreement with calculations based upon the assumption of valence neutrons together with core polarization. As one adds more valence protons and neutrons above ^{16}O, the 2p2h proton excitations move up in energy and the core-polarization contribution to the effective charges increase; for a ^{40}Ca core they are 0.56 for $1d-1d$ and 0.48 for $1d-2s$ neutrons [45]. The empirical value of 0.45 obtained in [44] should be attributed to effects of both core polarization and 2p2h proton excitations from the p to the sd shell. It is interesting to confirm whether these reduced effective charges can reproduce the B(E2) strength for ^{22}O. The latter has been measured in [50] with large uncertainties. New experiments aiming at constraining this value, e.g., [51], will thus add to our understanding of the oxygen isotopes.

The VS-IMSRG [6,7,54–57] provides a framework to produce ab initio valence-space Hamiltonians, based on NN+3N forces derived from chiral EFT. Working in a Hartree-Fock basis, we used the Magnus formulation of the IMSRG [6,7,58], to first decouple the ^{16}O core energy. Then we decoupled an sd-shell Hamiltonian, using the ensemble normal ordering procedure described in [56], to include effects of 3N forces between valence nucleons, specifically the five valence neutrons for the ^{21}O energies and transition rates. Finally, we used the approximate unitary transformation from the Magnus framework to additionally decouple an M1 or E2 valence-space operator consistent with the valence-space Hamiltonian [18]. In this framework, effective charges are thus not needed, but the effective operator is calculated consistently. Unless otherwise specified, all other technical details are the same as in [18,56]. The particular input NN+3N interaction used here, EM 1.8/2.0, was developed in [59,60].This interaction was generated by first performing a free-space SRG evolution [61] of the chiral N^{3}LO NN interaction of Entem and Machleidt [62] to 1.8 fm^{-1}, then adding a non-locally regulated N^{2}LO 3N interaction with cutoff 2.0 fm^{-1} with the low energy constants adjusted to reproduce the triton binding energy and the ^{4}He radius. This Hamiltonian, fit to few-body data, has been shown to reproduce ground- and excited-state energies across the nuclear chart from the p shell to the tin region [5,12,60,63,64]. Indeed, very good agreement between the experimental and VS-IMSRG excited-state energies is observed in Fig. 2. While E2 transition rates in the sd-shell are generally systematically below experiment, owing to the difficulty in capturing the highly collective physics of this transition, the trends typically agree well with experiment [20]. This can also be seen qualitatively

in Fig. 3, where the staggering of E2 strength resembles experiment. For the odd-mass cases, in particular ^{21}O, the agreement with experiment is rather good, while for the more collective transitions in even-mass isotopes the VS-IMSRG largely underestimates experiment.

We performed ab initio IM-NCSM calculations in the framework introduced in [65]. This novel method is a combination of the NCSM with a multi-reference IMSRG evolution of the many-body Hamiltonian that decouples a multi-determinantal reference state, typically an NCSM eigenstate from a small $N_{\max}^{\text{ref}} = 2$ reference space, from all Slater determinants outside of this reference space. The resulting Hamiltonian is employed in a final NCSM calculation to extract ground and excited states and all relevant observables. The decoupling leads to an extremely fast model-space convergence of the energies. For the application to electromagnetic observables in ^{21}O, two important developments beyond the basic IM-NCSM discussed in [65] were necessary: the consistent multi-reference in-medium evolution of the electromagnetic operators, as well as an extension to odd particle numbers via a particle-attachment or particle-removal scheme. The details of these extensions are presented in [66]. We performed IM-NCSM calculations with four different chiral NN+3N interactions to assess the sensitivity of our results to the input Hamiltonian: (i) the N^{2}LO$_{SAT}$ interaction [67]; (ii) the N^{3}LO$_{EM}$+N^{2}LO$_{L,400}$ interaction using the NN force of [62] in combination with a local 3N interaction at N^{2}LO with reduced cutoff [68]; (iii) the N^{3}LO$_{EM}$+N^{2}LO$_{NL,500}$ with the same NN force but an updated 3N interaction with a nonlocal regulator; and (iv) the N^{4}LO$_{EMN}$+N^{2}LO$_{NL,500}$ with a recent NN interaction at N^{4}LO [69] plus a 3N interaction at N^{2}LO with nonlocal regulator. The cutoff scale Λ, the low-energy constant c_D for the 3N interaction, and the SRG flow parameter α for the individual Hamiltonians were: (i) $\Lambda = 450$ MeV, $\alpha = 0.08$ fm^4, (ii) $\Lambda = 400$ MeV, $c_D = -0.2$, $\alpha = 0.08$ fm^4; (iii) $\Lambda = 500$ MeV, $c_D = 0.8$, $\alpha = 0.12$ fm^4; (iv) $\Lambda = 500$ MeV, $c_D = -1.8$, $\alpha = 0.16$ fm^4. We used the particle-removed calculation at the largest available $N_{\max} = 6$ as nominal result and the difference to the particle-attached calculations and the residual $N_{\max}$-dependence to quantify the uncertainty of the many-body calculation. Fig. 2 shows that the IM-NCSM calculations mostly provide a consistent description of the low-lying spectrum in very good agreement with experiment, except for the N^{2}LO$_{SAT}$ interaction. While the latter includes information beyond the few-body sector, particularly oxygen energies and radii, into the fit, it nonetheless produces a $1/2^+$ state over 1 MeV higher than experiment. The B(E2) transition strength from the first excited $1/2^+$ to the ground state, shown in Table 1, indicate interesting differences, even among the interactions that provide a consistent excitation spectrum. The N^{3}LO$_{EM}$+N^{2}LO$_{L,400}$ interaction using a local 3N regulator gives a significantly small B(E2) value compared to the other interactions that use nonlocal regulators. This shows that the E2 observables measured here pro-

vide a good test for chiral interactions that goes beyond the aspects probed by the excitation energies alone. A systematic study of the oxygen isotopes in the IM-NCSM is under way [70].

In summary, the low-lying structure of ^{21}O was studied at the NSCL using GRETINA coupled to the S800 spectrometer. The lifetime of the first (and second) excited state was measured for the first time, as well as γ-ray branching ratios from higher-lying states. Our experimental results are compared to ab initio VS-IMSRG and IM-NCSM predictions, demonstrating that E2 observables provide an interesting testing ground for chiral interactions and many-body methods that goes beyond the aspects probed by the excitation energies alone. Indeed, comparison of our experimental results with IM-NCSM calculations using different chiral NN+3N interactions suggests that interactions derived with nonlocal 3N regulators better capture the electromagnetic transition rates. Comparison of experiment with phenomenological shell model demonstrates that neutron-rich oxygen isotopes, and ^{21}O in particular, are prime candidates to study shell-model effective charges, since their low-lying structure should have relatively small contributions from 2p2h excitations.

Declaration of competing interest

The authors declare that they have no known competing financial interests or personal relationships that could have appeared to influence the work reported in this paper.

Acknowledgements

References

[1] E. Epelbaum, H.-W. Hammer, U.-G. Meißner, Modern theory of nuclear forces, Rev. Mod. Phys. 81 (2009) 1773.

[2] R. Machleidt, D. Entem, Chiral effective field theory and nuclear forces, Phys. Rep. 503 (1) (2011) 1–75, https://doi.org/10.1016/j.physrep.2011.02.001.

[3] G. Hagen, T. Papenbrock, M. Hjorth-Jensen, D.J. Dean, Coupled-cluster computations of atomic nuclei, Rep. Prog. Phys. 77 (9) (2014) 096302.

[4] C. Barbieri, A. Carbone, Self-consistent Green's function approaches, in: M. Hjorth-Jensen, M. Lombardo, U. van Kolck (Eds.), An Advanced Course in Computational Nuclear Physics, in: Lecture Notes in Physics, vol. 936, Springer, Cham, 2017.

[5] K. Hebeler, J.D. Holt, J. Menéndez, A. Schwenk, Nuclear forces and their impact on neutron-rich nuclei and neutron-rich matter, Annu. Rev. Nucl. Part. Sci. 65 (2015) 457.

[6] H. Hergert, S.K. Bogner, T.D. Morris, A. Schwenk, K. Tsukiyama, Phys. Rep. 621 (2016) 165–222.

[7] S.R. Stroberg, S.K. Bogner, H. Hergert, J.D. Holt, Non-empirical interactions for the nuclear shell model: an update, arXiv:1902.06154, 2019.

[8] J. Carlson, S. Gandolfi, F. Pederiva, S.C. Pieper, R. Schiavilla, K.E. Schmidt, R.B. Wiringa, Quantum Monte Carlo methods for nuclear physics, Rev. Mod. Phys. 87 (2015) 1067, https://doi.org/10.1103/RevModPhys.87.1067, arXiv:1412.3081.

[9] T. Otsuka, T. Suzuki, J.D. Holt, A. Schwenk, Y. Akaishi, Three-body forces and the limit of oxygen isotopes, Phys. Rev. Lett. 105 (2010) 032501, https://doi.org/10.1103/PhysRevLett.105.032501.

[10] H. Hergert, S. Binder, A. Calci, J. Langhammer, R. Roth, Ab initio calculations of even oxygen isotopes with chiral two-plus-three-nucleon interactions, Phys. Rev. Lett. 110 (2013) 242501, https://doi.org/10.1103/PhysRevLett.110.242501.

[11] A. Cipollone, C. Barbieri, P. Navrátil, Isotopic chains around oxygen from evolved chiral two- and three-nucleon interactions, Phys. Rev. Lett. 111 (2013) 062501, https://doi.org/10.1103/PhysRevLett.111.062501.

[12] J.D. Holt, S.R. Stroberg, A. Schwenk, J. Simonis, Ab initio limits of atomic nuclei, arXiv:1905.10475, 2019.

[13] J.D. Holt, J. Menéndez, A. Schwenk, Chiral three-nucleon forces and bound excited states in neutron-rich oxygen isotopes, Eur. Phys. J. A 49 (3) (2013) 39, https://doi.org/10.1140/epja/i2013-13039-2.

[14] C. Caesar, et al., Beyond the neutron drip-line: the unbound oxygen isotopes ^{25}O and ^{26}O, Phys. Rev. C 88 (3) (2013) 034313, https://doi.org/10.1103/PhysRevC.88.034313.

[15] S.K. Bogner, H. Hergert, J.D. Holt, A. Schwenk, S. Binder, A. Calci, J. Langhammer, R. Roth, Nonperturbative shell-model interactions from the in-medium similarity renormalization group, Phys. Rev. Lett. 113 (2014) 142501, https://doi.org/10.1103/PhysRevLett.113.142501.

[16] G.R. Jansen, J. Engel, G. Hagen, P. Navratil, A. Signoracci, Ab initio coupled-cluster effective interactions for the shell model: application to neutron-rich oxygen and carbon isotopes, Phys. Rev. Lett. 113 (2014) 142502, https://doi.org/10.1103/PhysRevLett.113.142502.

[17] P. Gysbers, et al., Discrepancy between experimental and theoretical β-decay rates resolved from first principles, Nat. Phys. 15 (5) (2019) 428, https://doi.org/10.1038/s41567-019-0450-7.

[18] N.M. Parzuchowski, S.R. Stroberg, P. Navrátil, H. Hergert, S.K. Bogner, Ab initio electromagnetic observables with the in-medium similarity renormalization group, Phys. Rev. C 96 (2017) 034324, https://doi.org/10.1103/PhysRevC.96.034324.

[19] R.F. Garcia Ruiz, et al., Ground-state electromagnetic moments of calcium isotopes, Phys. Rev. C 91 (2015) 041304, https://doi.org/10.1103/PhysRevC.91.041304.

[20] J. Henderson, G. Hackman, P. Ruotsalainen, S. Stroberg, K. Launey, J. Holt, F. Ali, N. Bernier, M. Bentley, M. Bowry, et al., Testing microscopically derived descriptions of nuclear collectivity: Coulomb excitation of ^{22}Mg, Phys. Lett. B 782 (2018) 468–473, https://doi.org/10.1016/j.physletb.2018.05.064.

[21] A. Klose, K. Minamisono, A.J. Miller, B.A. Brown, D. Garand, J.D. Holt, J.D. Lantis, Y. Liu, B. Maaß Nörtershäuser, et al., Ground-state electromagnetic moments of ^{37}Ca, Phys. Rev. C 99 (2019) 061301, https://doi.org/10.1103/PhysRevC.99.061301.

[22] S. Bacca, S. Pastore, Electromagnetic reactions on light nuclei, J. Phys. G 41 (12) (2014) 123002, https://doi.org/10.1088/0954-3899/41/12/123002, arXiv:1407.3490.

[23] M. Stanoiu, F. Azaiez, Z. Dombrádi, O. Sorlin, B.A. Brown, M. Belleguic, D. Sohler, M.G. Saint Laurent, M.J. Lopez-Jimenez, Y.E. Penionzhkevich, et al., $N = 14$ and 16 shell gaps in neutron-rich oxygen isotopes, Phys. Rev. C 69 (2004) 034312, https://doi.org/10.1103/PhysRevC.69.034312.

[24] D. Morrissey, B. Sherrill, M. Steiner, A. Stolz, I. Wiedenhoever, Commissioning the A1900 projectile fragment separator, Nucl. Instrum. Methods Phys. Res., Sect. B, Beam Interact. Mater. Atoms 204 (2003) 90–96, https://doi.org/10.1016/S0168-583X(02)01895-5.

[25] D. Morrissey, et al., A new high-resolution separator for high-intensity secondary beams, Nucl. Instrum. Methods Phys. Res., Sect. B, Beam Interact. Mater. Atoms 126 (1) (1997) 316–319, https://doi.org/10.1016/S0168-583X(96)01003-8.

[26] D. Bazin, J. Caggiano, B. Sherrill, J. Yurkon, A. Zeller, The S800 spectrograph, Nucl. Instrum. Methods Phys. Res., Sect. B, Beam Interact. Mater. Atoms 204 (2003) 629–633, https://doi.org/10.1016/S0168-583X(02)02142-0.

[27] S. Paschalis, I. Lee, A. Macchiavelli, C. Campbell, M. Cromaz, S. Gros, J. Pavan, J. Qian, R. Clark, H. Crawford, et al., The performance of the gamma-ray energy tracking in-beam nuclear array GRETINA, Nucl. Instrum. Methods Phys. Res., Sect. A, Accel. Spectrom. Detect. Assoc. Equip. 709 (2013) 44–55, https://doi.org/10.1016/j.nima.2013.01.009.

[28] D. Weisshaar, D. Bazin, P. Bender, C. Campbell, F. Recchia, V. Bader, T. Baugher, J. Belarge, M. Carpenter, H. Crawford, et al., The performance of the gamma-ray tracking array GRETINA for gamma-ray spectroscopy with fast beams of rare isotopes, Nucl. Instrum. Methods Phys. Res., Sect. A, Accel. Spectrom. Detect. Assoc. Equip. 847 (2017) 187–198, https://doi.org/10.1016/j.nima.2016.12.001.

[29] H. Iwasaki, A. Dewald, T. Braunroth, C. Fransen, D. Smalley, A. Lemasson, C. Morse, K. Whitmore, C. Loelius, The triple plunger for exotic beams triplex for excited-state lifetime measurement studies on rare isotopes, Nucl. Instrum. Methods Phys. Res., Sect. A, Accel. Spectrom. Detect. Assoc. Equip. 806 (2016) 123–131, https://doi.org/10.1016/j.nima.2015.09.091.

[30] J.R. Terry, B.A. Brown, C.M. Campbell, J.M. Cook, A.D. Davies, D.-C. Dinca, A. Gade, T. Glasmacher, P.G. Hansen, B.M. Sherrill, et al., Single-neutron knockout

from intermediate energy beams of ^{30,32}Mg: mapping the transition into the "island of inversion", Phys. Rev. C 77 (2008) 014316, https://doi.org/10.1103/PhysRevC.77.014316.

[31] P. Doornenbal, P. Reiter, H. Grawe, T. Saito, A. Al-Khatib, A. Banu, T. Beck, F. Becker, P. Bednarczyk, G. Benzoni, et al., Lifetime effects for high-resolution gamma-ray spectroscopy at relativistic energies and their implications for the RISING spectrometer, Nucl. Instrum. Methods Phys. Res., Sect. A, Accel. Spectrom. Detect. Assoc. Equip. 613 (2) (2010) 218–225, https://doi.org/10.1016/j.nima.2009.11.017.

[32] C. Domingo-Pardo, D. Bazzacco, P. Doornenbal, E. Farnea, A. Gadea, J. Gerl, H. Wollersheim, Conceptual design and performance study for the first implementation of AGATA at the in-flight rib facility of gsi, Nucl. Instrum. Methods Phys. Res., Sect. A, Accel. Spectrom. Detect. Assoc. Equip. 694 (2012) 297–312, https://doi.org/10.1016/j.nima.2012.08.039.

[33] K. Whitmore, D. Smalley, H. Iwasaki, T. Suzuki, V.M. Bader, D. Bazin, J.S. Berryman, B.A. Brown, C.M. Campbell, P. Fallon, et al., Magnetic response of the halo nucleus ^{19}C studied via lifetime measurement, Phys. Rev. C 91 (2015) 041303, https://doi.org/10.1103/PhysRevC.91.041303.

[34] A. Chester, P. Adrich, A. Becerril, D. Bazin, C. Campbell, J. Cook, D.-C. Dinca, W. Mueller, D. Miller, V. Moeller other, Application of the time-of-flight technique for lifetime measurements with relativistic beams of heavy nuclei, Nucl. Instrum. Methods Phys. Res., Sect. A, Accel. Spectrom. Detect. Assoc. Equip. 562 (1) (2006) 230–240, https://doi.org/10.1016/j.nima.2006.02.182.

[35] P. Adrich, D. Enderich, D. Miller, V. Moeller, R. Norris, K. Starosta, C. Vaman, P. Voss, A. Dewald, A simulation tool for recoil distance method lifetime measurements at nscl, Nucl. Instrum. Methods Phys. Res., Sect. A, Accel. Spectrom. Detect. Assoc. Equip. 598 (2) (2009) 454–464, https://doi.org/10.1016/j.nima.2008.09.055.

[36] K. Starosta, A. Dewald, A. Dunomes, P. Adrich, A.M. Amthor, T. Baumann, D. Bazin, M. Bowen, B.A. Brown, A. Chester, et al., Shape and structure of $n = z$ ^{64}Ge: electromagnetic transition rates from the application of the recoil distance method to a knockout reaction, Phys. Rev. Lett. 99 (2007) 042503, https://doi.org/10.1103/PhysRevLett.99.042503.

[37] M. Petri, P. Fallon, A.O. Macchiavelli, S. Paschalis, K. Starosta, T. Baugher, D. Bazin, L. Cartegni, R.M. Clark, H.L. Crawford, et al., Lifetime measurement of the 2_1^+ state in ^{20}C, Phys. Rev. Lett. 107 (2011) 102501, https://doi.org/10.1103/PhysRevLett.107.102501.

[38] M. Petri, S. Paschalis, R.M. Clark, P. Fallon, A.O. Macchiavelli, K. Starosta, T. Baugher, D. Bazin, L. Cartegni, H.L. Crawford, et al., Structure of ^{16}C: testing shell model and ab initio approaches, Phys. Rev. C 86 (2012) 044329, https://doi.org/10.1103/PhysRevC.86.044329.

[39] S. Agostinelli, J. Allison, K. Amako, J. Apostolakis, H. Araujo, P. Arce, M. Asai, D. Axen, S. Banerjee, G. Barrand, et al., Geant4 – a simulation toolkit, Nucl. Instrum. Methods Phys. Res., Sect. A, Accel. Spectrom. Detect. Assoc. Equip. 506 (3) (2003) 250–303, https://doi.org/10.1016/S0168-9002(03)01368-8.

[40] C.S. Sumithrarachchi, D.J. Morrissey, A.D. Davies, D.A. Davies, M. Facina, E. Kwan, P.F. Mantica, M. Portillo, Y. Shimbara, J. Stoker, et al., States in ^{22}O via β decay of ^{22}N, Phys. Rev. C 81 (2010) 014302, https://doi.org/10.1103/PhysRevC.81.014302.

[41] Z.H. Li, J.L. Lou, Y.L. Ye, H. Hua, D.X. Jiang, X.Q. Li, S.Q. Zhang, T. Zheng, Y.C. Ge, Z. Kong, et al., Experimental study of the β-delayed neutron decay of ^{21}N, Phys. Rev. C 80 (2009) 054315, https://doi.org/10.1103/PhysRevC.80.054315.

[42] D. Ralet, S. Pietri, T. Rodríguez, M. Alaqeel, T. Alexander, N. Alkhomashi, F. Ameil, T. Arici, A. Ataç, R. Avigo, et al., Lifetime measurement of neutron-rich even-even molybdenum isotopes, Phys. Rev. C 95 (2017) 034320, https://doi.org/10.1103/PhysRevC.95.034320.

[43] B.A. Brown, W.A. Richter, New "USD" Hamiltonians for the sd shell, Phys. Rev. C 74 (2006) 034315, https://doi.org/10.1103/PhysRevC.74.034315.

[44] W.A. Richter, S. Mkhize, B.A. Brown, sd-shell observables for the usda and usdb Hamiltonians, Phys. Rev. C 78 (2008) 064302, https://doi.org/10.1103/PhysRevC.78.064302.

[45] B. Brown, A. Arima, J. McGrory, E2 core-polarization charge for nuclei near 16O and 40Ca, Nucl. Phys. A 277 (1) (1977) 77–108, https://doi.org/10.1016/0375-9474(77)90263-9.

[46] F. Raimondi, C. Barbieri, Core-polarization effects and effective charges in O and Ni isotopes from chiral interactions, Phys. Rev. C 100 (2019) 024317, https://doi.org/10.1103/PhysRevC.100.024317.

[47] H.T. Fortune, Concerning positive-parity collective states in ^{18}O, The European Physical Journal A 48 (5) (2012) 63, https://doi.org/10.1140/epja/i2012-12063-0.

[48] S. LaFrance, H.T. Fortune, S. Mordechai, M.E. Cobern, G.E. Moore, R. Middleton, W. Chung, B.H. Wildenthal, ^{20}O from ^{18}O(t,p), Phys. Rev. C 20 (1979) 1673–1679, https://doi.org/10.1103/PhysRevC.20.1673.

[49] E.K. Warburton, B.A. Brown, Effective interactions for the 0p1s0d nuclear shell-model space, Phys. Rev. C 46 (1992) 923–944, https://doi.org/10.1103/PhysRevC.46.923.

[50] P.G. Thirolf, B.V. Pritychenko, B.A. Brown, P.D. Cottle, M. Chromik, T. Glasmacher, G. Hackman, R.W. Ibbotson, K.W. Kemper, T. Otsuka, et al., Spectroscopy of the 2_1^+ state in ^{22}O and shell structure near the neutron drip line, Phys. Lett. B 485 (1) (2000) 16–22.

[51] M. Petri, et al., ANL Propos. 1732 (2018).

[52] D. Tilley, H. Weller, C. Cheves, R. Chasteler, Energy levels of light nuclei A = 18–19, Nucl. Phys. A 595 (1) (1995) 1–170.

[53] B. Pritychenko, M. Birch, B. Singh, M. Horoi, Tables of E2 transition probabilities from the first 2^+ states in even–even nuclei, At. Data Nucl. Data Tables 107 (2016) 1–139.

[54] K. Tsukiyama, S.K. Bogner, A. Schwenk, In-medium similarity renormalization group for open-shell nuclei, Phys. Rev. C 85 (2012) 061304(R).

[55] S.K. Bogner, H. Hergert, J.D. Holt, A. Schwenk, S. Binder, A. Calci, J. Langhammer, R. Roth, Nonperturbative shell-model interactions from the in-medium similarity renormalization group, Phys. Rev. Lett. 113 (2014) 142501, https://doi.org/10.1103/PhysRevLett.113.142501.

[56] S.R. Stroberg, A. Calci, H. Hergert, J.D. Holt, S.K. Bogner, R. Roth, A. Schwenk, Nucleus-dependent valence-space approach to nuclear structure, Phys. Rev. Lett. 118 (2017) 032502, https://doi.org/10.1103/PhysRevLett.118.032502.

[57] S.R. Stroberg, H. Hergert, J.D. Holt, S.K. Bogner, A. Schwenk, Ground and excited states of doubly open-shell nuclei from ab initio valence-space Hamiltonians, Phys. Rev. C 93 (2016) 051301, https://doi.org/10.1103/PhysRevC.93.051301.

[58] T.D. Morris, N.M. Parzuchowski, S.K. Bogner, Magnus expansion and in-medium similarity renormalization group, Phys. Rev. C 92 (2015) 034331, https://doi.org/10.1103/PhysRevC.92.034331.

[59] K. Hebeler, S.K. Bogner, R.J. Furnstahl, A. Nogga, A. Schwenk, Improved nuclear matter calculations from chiral low-momentum interactions, Phys. Rev. C 83 (2011) 031301, https://doi.org/10.1103/PhysRevC.83.031301.

[60] J. Simonis, S.R. Stroberg, K. Hebeler, J.D. Holt, A. Schwenk, Saturation with chiral interactions and consequences for finite nuclei, Phys. Rev. C 96 (2017) 014303, https://doi.org/10.1103/PhysRevC.96.014303.

[61] S.K. Bogner, R.J. Furnstahl, R.J. Perry, Phys. Rev. C 75 (2007) 061001.

[62] D.R. Entem, R. Machleidt, Accurate charge-dependent nucleon-nucleon potential at fourth order of chiral perturbation theory, Phys. Rev. C 68 (2003) 041001, https://doi.org/10.1103/PhysRevC.68.041001.

[63] T.D. Morris, J. Simonis, S.R. Stroberg, C. Stumpf, G. Hagen, J.D. Holt, G.R. Jansen, T. Papenbrock, R. Roth, A. Schwenk, Structure of the lightest tin isotopes, Phys. Rev. Lett. 120 (2018) 152503, https://doi.org/10.1103/PhysRevLett.120.152503.

[64] R. Taniuchi, C. Santamaria, P. Doornenbal, A. Obertelli, K. Yoneda, G. Authelet, H. Baba, D. Calvet, F. Château, A. Corsi, et al., Nature 569 (7754) (2019) 53–58.

[65] E. Gebrerufael, K. Vobig, H. Hergert, R. Roth, Ab initio description of open-shell nuclei: merging no-core shell model and in-medium similarity renormalization group, Phys. Rev. Lett. 118 (2017) 152503, https://doi.org/10.1103/PhysRevLett.118.152503.

[66] K. Vobig, R. Roth, 2020, in preparation.

[67] A. Ekström, G.R. Jansen, K.A. Wendt, G. Hagen, T. Papenbrock, B.D. Carlsson, C. Forssén, M. Hjorth-Jensen, W. Navrátil, W. Nazarewicz, Accurate nuclear radii and binding energies from a chiral interaction, Phys. Rev. C 91 (2015) 051301, https://doi.org/10.1103/PhysRevC.91.051301.

[68] R. Roth, S. Binder, K. Vobig, A. Calci, J. Langhammer, P. Navrátil, Medium-mass nuclei with normal-ordered chiral $NN+3N$ interactions, Phys. Rev. Lett. 109 (2012) 052501, https://doi.org/10.1103/PhysRevLett.109.052501.

[69] D.R. Entem, R. Machleidt, Y. Nosyk, High-quality two-nucleon potentials up to fifth order of the chiral expansion, Phys. Rev. C 96 (2017) 024004, https://doi.org/10.1103/PhysRevC.96.024004.

[70] R. Roth, et al., 2020, in preparation.